Nanoparticles reveal that human cervicovaginal mucus is riddled with pores larger than viruses

Samuel K. Lai[a,b], Ying-Ying Wang[c], Kaoru Hida[c], Richard Cone[d,b], and Justin Hanes[a,c,b,1]

[a]Department of Chemical and Biomolecular Engineering, [c]Department of Biomedical Engineering, [d]Department of Biophysics, and [b]Institute for NanoBioTechnology, Johns Hopkins University, 3400 N. Charles Street, Baltimore, MD 21218

Edited by Robert Langer, Massachusetts Institute of Technology, Cambridge, MA, and approved November 6, 2009 (received for review October 10, 2009)

The mechanisms by which mucus helps prevent viruses from infecting mucosal surfaces are not well understood. We engineered non-mucoadhesive nanoparticles of various sizes and used them as probes to determine the spacing between mucin fibers (pore sizes) in fresh undiluted human cervicovaginal mucus (CVM) obtained from volunteers with healthy vaginal microflora. We found that most pores in CVM have diameters significantly larger than human viruses (average pore size 340 ± 70 nm; range approximately 50–1800 nm). This mesh structure is substantially more open than the 15–100-nm spacing expected assuming mucus consists primarily of a random array of individual mucin fibers. Addition of a nonionic detergent to CVM caused the average pore size to decrease to 130 ± 50 nm. This suggests hydrophobic interactions between lipid-coated "naked" protein regions on mucins normally cause mucin fibers to self-condense and/or bundle with other fibers, creating mucin "cables" at least three times thicker than individual mucin fibers. Although the native mesh structure is not tight enough to trap most viruses, we found that herpes simplex virus (approximately 180 nm) was strongly trapped in CVM, moving at least 8,000-fold slower than non-mucoadhesive 200-nm nanoparticles. This work provides an accurate measurement of the pore structure of fresh, hydrated ex vivo CVM and demonstrates that mucoadhesion, rather than steric obstruction, may be a critical protective mechanism against a major sexually transmitted virus and perhaps other viruses.

cervicovaginal tract | herpes simplex virus | hydrophobic interactions | microstructure | particle tracking

Mucus forms a continuously renewed, semipermeable viscoelastic barrier that coats all mucosal surfaces of the body, including those of the eyes and the respiratory, gastrointestinal, and female reproductive tracts (1–3). Mucus helps to protect these surfaces from infection and injury, but pathogens and toxic particles that are able to penetrate the mucus coat may more readily harm the underlying tissue (3, 4). At the nanoscale, mucus is a heterogeneous mesh network of mucin fibers in a low-viscosity (watery) interstitial fluid (5–9). It is generally believed that mucus gels sterically exclude pathogens and other particles that are larger than the effective pore sizes in the mesh network. The view that mucus protects by steric exclusion was supported by a prior investigation, which demonstrated that small virus-like particles consisting of the capsids of Norwalk virus (38 nm) and human papilloma virus (HPV; 55 nm) diffused through human ovulatory cervical mucus (OCM) at the same speeds at which they diffuse through water, while a larger enveloped virus, herpes simplex virus (HSV; 180 nm), was greatly slowed (8). Assuming that HSV was stopped by steric obstruction, the authors estimated the average pore size of human OCM to be approximately 100 nm (the approximate size of many human viruses).

Despite major advances in elucidating the biochemical structure of mucin fibers and 30 years of microscopic observations of mucus gels, the microstructure or pore size of mucus gels in their native, hydrated state remains uncertain. Electron microscopy of human cervical mucus has produced a wide range of pore size estimates depending on the methods used, from approximately 100 nm by using SEM (10) or DMSO-mediated glutaraldehyde fixation and transmission electron microscopy (TEM) (8), to 500–800 nm by using freeze substitution and TEM (11), and even 1,000–10,000 nm or larger by using various conventional EM procedures (12–14).

We reasoned that the thermal motions of non-mucoadhesive nanoparticles could reveal the microstructure of mucus as experienced by virus-sized objects and that these probe particles could be introduced into fresh, native mucus samples with minimal perturbation. As particle size increases to approach the mucus pore size, steric obstruction should increasingly restrict the free diffusion of the probe particles. This approach requires, however, that nanoprobes be engineered to avoid adhesive interactions with mucus (1, 8, 15, 16), making them unsuitable as probes of mucus microstructure. To address this problem, we recently engineered nanoparticles densely coated with low molecular weight polyethylene glycol (PEG) and showed that they do not adhere to mucus (6, 17). Here, we use non-mucoadhesive nanoparticles to provide a reliable estimate of pore sizes in fresh, minimally perturbed human cervicovaginal mucus (CVM). We then show that CVM provides protection against HSV penetration not by steric obstruction, but rather by highly effective adhesive interactions.

Results

Mucus Pores Are Much Larger Than Predicted by Mucin Fiber Diameter and Concentration. We added fluorescent, non-mucoadhesive (i.e., densely coated with PEG) nanoparticles to fresh, undiluted human CVM obtained from donors with healthy vaginal microflora and quantified the particle motions by using high-resolution multiple-particle tracking (MPT) (6, 18). PEG-coated 100-, 200-, and 500-nm particles rapidly penetrated mucus, with geometric ensemble mean squared displacements ($\langle MSD \rangle$) that were 6,000-, 600-, and 400-fold higher, respectively, than uncoated (mucoadhesive) particles of the same size (Fig. 1*A*) (6). The non-mucoadhesive surface of PEG-coated particles resulted in ensemble effective diffusivities at a time scale of 1 s that were only 6.5-, 3.5-, and 12- fold lower than those for the same particles in water, respectively. In contrast, the diffusivity of 1-μm PEG-coated particles in mucus was approximately 200-fold slower than in water (Fig. S1), likely due to significant steric obstruction by mucus mesh elements.

To determine the effective size of pores in mucus, we fitted the measured diffusion rates of probe particles to Amsden's obstruction-scaling model (19, 20) for entangled and cross-linked gels (8, 21). We found that the average pore size of minimally perturbed human CVM is at least 340 ± 70 nm, with a broad

Author contributions: S.K.L., Y.-Y.W., R.C., and J.H. designed research; S.K.L., Y.-Y.W., and K.H. performed research; S.K.L., Y.-Y.W., and K.H. analyzed data; and S.K.L., Y.-Y.W., R.C., and J.H. wrote the paper.

The authors declare no conflict of interest.

This article is a PNAS Direct Submission.

[1]To whom correspondence should be addressed. E-mail: hanes@jhu.edu.

This article contains supporting information online at www.pnas.org/cgi/content/full/0911748107/DCSupplemental.

www.pnas.org/cgi/doi/10.1073/pnas.0911748107

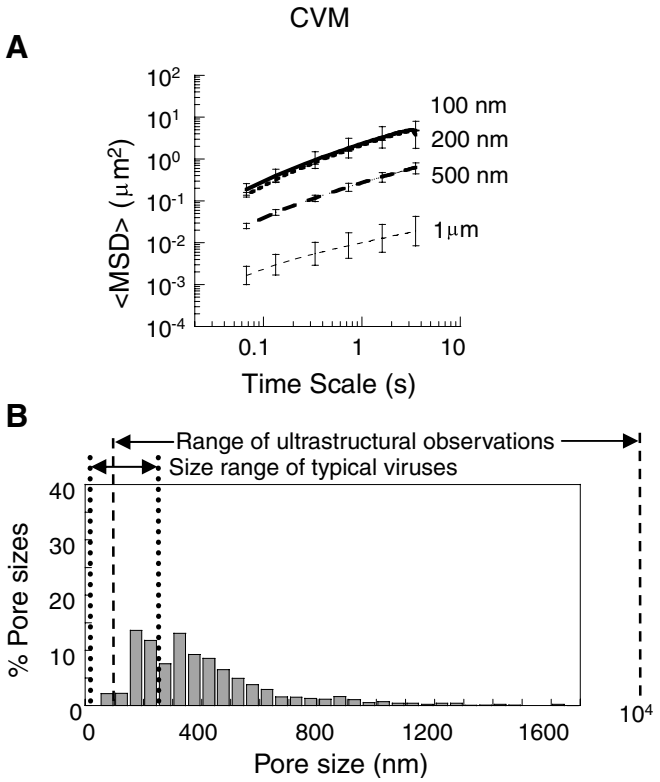

Fig. 1. Transport of different-sized PEG-coated particles in minimally perturbed human CVM. (*A*) Ensemble-averaged geometric mean squared displacements (⟨MSD⟩) as a function of time scale. Error bars are presented as standard error of the mean (s.e.m). (*B*) Distribution of effective pore sizes, with average pore size 340 ± 70 nm (s.e.m.). Data represent the ensemble average of at least three independent experiments, with $n \geq 120$ particles for each experiment.

distribution (Fig. 1*B*). The largest 10% of pore sizes experienced by the particles were >750 nm, whereas the smallest pores were no larger than 50 nm. Overall, approximately 25% of the pores sampled by probe particles were larger than 500 nm and more than 80% were larger than 200 nm.

Mucins are long, flexible and highly glycosylated proteins, with a fiber diameter of 5–10 nm based on their biochemical structure and as confirmed by both negatively stained electron microscopic images of individual mucin fibers (22, 23) and by the DMSO-mediated glutaraldehyde fixation method (1). The concentration of mucins in mucus gels typically ranges between 1–5% (1, 24–28). Based on these values, a cubic lattice model that assumes mucins to be long rigid polymers predicts an average pore size of 40–100 nm. If mucins are instead assumed to be flexible polymers (29, 30), the predicted pore size is approximately 15–50 nm (31). Therefore, the rapid diffusion of 500-nm PEG-coated nanoparticles indicates that individual mucin monomers must be condensed and/or bundled together into thick cables in CVM, markedly increasing the pore size. Based on lattice modeling, the average pore size of 340 nm measured here implies that mucin cables in CVM are, on average, 3–6 times thicker than the approximately 10-nm diameter of a single mucin fiber.

CVM Mucins Are Condensed and/or Bundled into Thick Cables via Hydrophobic Interactions. Mucins have short hydrophobic domains (lipid-coated, nonglycosylated, cysteine-rich domains) interspersed between long glycosylated regions (5, 32). The negatively charged glycosylated domains likely repel each other, but the hydrophobic domains may cause mucins to self-condense and/or bundle together (33–35). To test this, we added 1% vol/vol of a nonionic detergent, (nonylphenoxy)polyethylene oxide, to the same mucus samples and again characterized the pore size. Addition of this detergent had no effect on the diffusion rate of the 100-nm probe particles, but markedly decreased the diffusion rates of 200- and 500-nm probe particles, by 160- and 140-fold, respectively (Figs. 2*A* and S2). Addition of the same volume of PBS instead of the detergent did not affect particle motion in mucus. The average pore size after detergent treatment was 130 ± 50 nm, with a much narrower distribution than in native mucus (Fig. 2*B*). The percentage of pores larger than 200 nm decreased from >80% in unmodified CVM to <15% in detergent-treated CVM. Thus, treatment of mucus with a nonionic detergent strongly debundled the mucins, suggesting that the condensation and bundling of mucin fibers to form thick cables in unmodified CVM is largely driven by hydrophobic interactions.

Mucoadhesion, Not Steric Obstruction, Traps HSV in CVM. Most mammalian viruses are substantially smaller than the average pore size of CVM measured here, suggesting that mucus gels are unlikely to block virus penetration by steric obstruction as previously speculated. However, viruses and particles smaller than the pores can be trapped by adhesive interactions with the mucus gel. We investigated the translational motions of HSV (diameter approximately 180 nm) in CVM and compared its motions with those of 200-nm PEG-coated particles. The diffusion of HSV was strongly hindered in CVM obtained from women with healthy vaginal microflora (Fig. 3*A*). In fact, HSV was essentially trapped, moving at least 8,000 times slower than the slightly larger mucus-penetrating nanoparticles in CVM (Fig. 3*B*) and 20,000-fold slower than HSV diffuses through water. The degree of HSV

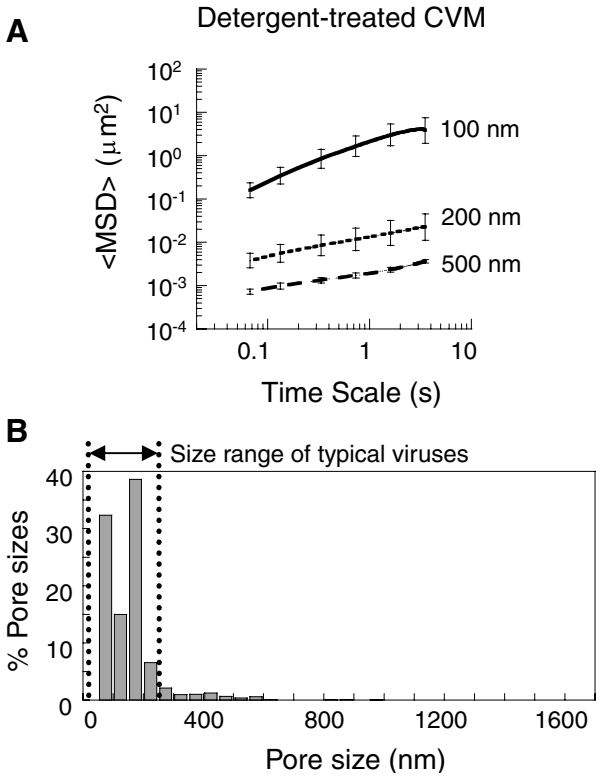

Fig. 2. Transport of different-sized PEG-coated particles in detergent-treated human CVM. (*A*) Ensemble-averaged geometric mean squared displacements (⟨MSD⟩) as a function of time scale. Error bars are presented as s.e.m. (*B*) Distribution of effective pore sizes, with average pore size 130 ± 50 nm (s.e.m.). Data represent the ensemble average of at least three independent experiments, with $n \geq 120$ particles for each experiment.

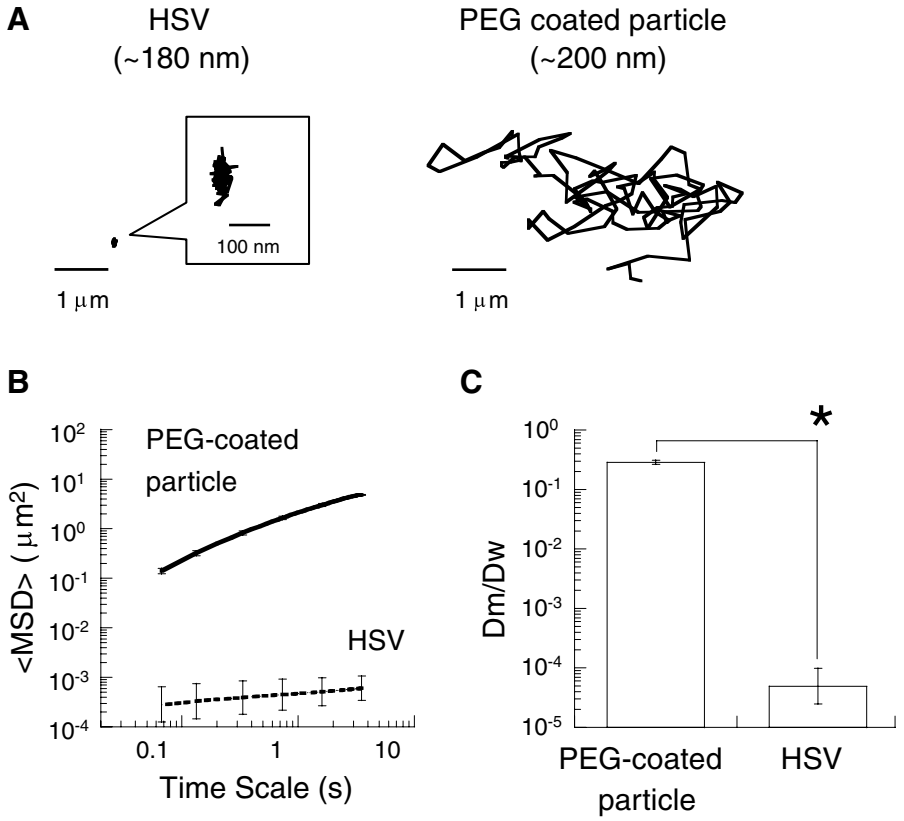

Fig. 3. Transport of HSV (diameter 180 nm) in minimally perturbed human cervicovaginal mucus compared to 200-nm non-mucoadhesive, PEG-coated particles. (*A*) Representative trajectories of HSV and 200-nm PEG-coated particles, with effective diffusivities within one s.e.m. of their ensemble average. (*B*) Ensemble-averaged geometric mean squared displacements (⟨MSD⟩) as a function of time scale. (*C*) Ratios of the ensemble average diffusion coefficients in mucus (D_m) compared to in water (D_w). Data represent three independent experiments for HSV, with $n \geq 100$ virus particles tracked for each experiment. The asterisk (*) indicates statistical significance ($P < 0.005$). Error bars are presented as s.e.m.

trapping by mucus, reflected by the time-lapse traces of individual virions, was comparable to that of uncoated polystyrene particles, which are essentially permanently immobilized in CVM by polyvalent adhesive interactions. Similarly, the α value, which reflects the extent of impediment to free diffusion ($\alpha = 1$ for free diffusion; $\alpha < 1$ indicates increasing impediment to particle movement as α decreases; see *Methods*) (6), was 0.18 for HSV compared to 0.16 and 0.36 for 100- and 200-nm polystyrene particles, respectively (6). These results indicate that HSV is trapped by mucoadhesion rather than by steric obstruction (Fig. 3*C*).

Discussion

The extent and mechanisms by which mucus secretions protect against pathogen penetration are largely unknown. Previous work, based on the transport rates of various viruses, estimated the average pore size of OCM to be approximately 100 nm (8). This expectation was supported by the approximately 100-nm pore size indicated by electron microscopy of OCM by using DMSO-mediated glutaraldehyde fixation (1), the only fixation method that yields images consistent with the approximately 10-nm fiber diameter expected from the well-established biochemical structure of individual mucin fibers. It was also supported by the observation that HSV, a virus with a diameter (180 nm) substantially larger than 100 nm, was immobilized in human OCM (8). The 10- to 100-fold higher mucin content in CVM and other mucus secretions compared to OCM (1) was expected to lead to pores that are substantially smaller than those found in OCM, and therefore smaller than most viruses. However, our results suggest that mucin fibers in CVM must be condensed and/or bundled together to form thick cables that create large pores on the order of hundreds of nanometers. With pores so large, CVM is not likely to block most viruses by steric obstruction. Thus, to form a substantial protective barrier against viruses, the mucus gel must instead trap them by adhesive interactions. We find that CVM almost certainly traps HSV (180 nm) by adhesive interactions because larger, non-mucoadhesive nanoparticles (200 and 500 nm) diffuse through CVM at markedly faster rates (10^3- to 10^4-fold difference). We have also recently discovered that cell-free HIV (120 nm) is trapped in acidic CVM (36), providing another example of a virus whose diffusion is most likely slowed or stopped by adhesive interactions with mucus.

In contrast to HSV, virus-like particles consisting of the capsids of Norwalk virus and HPV diffuse through human OCM as fast as they diffuse through water (8). These capsid viruses are small enough to fit into the large pores in CVM, and likely avoid mucoadhesive interactions by having surfaces that are densely populated with equal numbers of positive and negative charge groups (yielding a net neutral charge) as well as by having minimal to no exposed hydrophobic surfaces that might adhere to the lipid-coated "naked protein" domains of mucins (1). The mechanism by which HSV is adhesively trapped in mucus remains unclear; however, HSV is an enveloped virus with a surface that is expected to be more hydrophobic than that of small capsid viruses (1, 37). We previously found that hydrophobic interactions between particles and mucus are sufficiently avid to strongly impede the motions of latex particles with diameters of 59–1000 nm (6, 8). Indeed, at high particle concentrations, hydrophobic interactions can cause mucin fibers to aggregate about and thereby permanently trap the particles (8). In this study, the immobility

of HSV is unlikely a byproduct of a high particle concentration, because we used a virus concentration several orders of magnitude lower than the concentration of uncoated latex particles necessary to collapse mucus fibers. We observed a uniform distribution of HSV particles in CVM with no aggregation of fluorescence, a hallmark of particle-induced mucin aggregation (8).

Numerous electron microscopy observations have indicated that mucus gel structures consist of cables much thicker than individual mucin fibers, with pore sizes that vary over a 100-fold range (approximately 100 nm to over 10,000 nm) depending on the method of sample preparation as well as the source of mucus. This sensitivity to the preparation method suggests that mucus gels can be altered by methods that require dehydration and/or fixation, such as electron microscopy. Instead, determining the effective pore size as experienced by viruses and nanoparticles requires methods that minimally perturb mucus samples. The pore size we observe in CVM is most consistent with electron microscopy images of human OCM obtained by using a snap-freeze (liquid Freon at 170 °C) followed by a freeze-substitution fixation method (11). This appears to be the only published method that preserves a similar degree of mucin fiber condensation and/or bundling as what we infer from the diffusion rates of mucus-penetrating nanoparticles.

That a nonionic detergent markedly reduced the pore size in CVM suggests that the hydrophobic domains of mucins cause them to condense and/or bundle into thick cables. Surprisingly, we found that the addition of the nonionic detergent did not significantly alter the macroscopic viscoelastic properties of CVM (31). Thus, mucus pore size may be modulated independently of mucus macroscopic viscoelasticity. These results suggest that topical applications of surface-active agents might be used to alter the effective pore size for therapeutic or prophylactic purposes without altering the bulk viscoelastic characteristics critical for mucus transport mechanisms (e.g., mucociliary and peristaltic transport) (1, 38–41). Numerous vaginal microbicides that have been tested in humans possess strong surfactant properties and, therefore, may also alter mucus pore size. However, most of these agents caused substantial toxicity to the vaginal epithelium by damaging cell membranes, and therefore failed to reduce (or in some cases even increased) infection rates (42–45). Thus, whereas our results suggest that the use of surface-active agents may help limit infection by decreasing the flux of pathogens to the epithelium, this hypothesis can only be tested with agents that do not simultaneously compromise the epithelial cell layer.

Bundling of mucin fibers may be critical for the ability of mucus to maintain its bulk rheological properties in response to shear over large distances. In particular, mucin–mucin adhesive interactions (that cause bundling) may be important for rapid recovery of the bulk viscoelasticity of polymer gels after a large strain (1, 46). Multiple hydrophobic interactions between mucin fibers may therefore enable mucus to be cleared efficiently by cough clearance (slower recovery of elasticity, which may occur in the absence of these adhesive interactions, might cause mucus to drip back into the lungs). Rapid recovery of elasticity likely also helps to maintain good lubrication properties during repeated large strains, as in rapid eye blinking and copulation. Finally, previous work by Matsui et al. has demonstrated that the increased viscoelasticity and/or reduced pore size of dehydrated airway mucus, such as in cystic fibrosis (47), effectively prevent the migration of neutrophils, perhaps partly explaining the persistence of bacterial infections in CF patients (48).

Mucosally transmitted pathogens must penetrate the mucus barrier to infect target cells. Our result that HSV is strongly trapped in CVM from women with healthy, lactobacilli-dominated vaginal microflora suggests "healthy" CVM offers considerable protection against HSV penetration to the underlying epithelium. However, the seroprevalence of HSV-2 (commonly associated with genital transmission) is as high as 25% among sexually active adults in the US (49) and substantially higher in developing countries (50). A plausible explanation for this paradox is that the capacity of healthy CVM to adhesively trap HSV and other pathogens may be compromised by physicochemical alterations to the mucus gel. Only about 40% of sexually active women in the US have healthy vaginal microflora, whereas the remainder of women experience an overgrowth in anaerobic bacteria, resulting in intermediate microflora or bacterial vaginosis (BV) (51). BV is characterized by high concentrations of mucin-degrading enzymes and more watery (low viscoelasticity) cervicovaginal secretions (52). Importantly, women with BV are at markedly increased risks of infection by various sexually transmitted pathogens, such as HIV-1 (53, 54) and HSV-2 (55). Thus, adhesive trapping of pathogens in CVM may be substantially reduced in women with BV or intermediate microflora. It also remains to be established whether adhesive trapping of viruses may be compromised when seminal fluids are mixed with CVM. Studies of virus transport in midcycle (ovulatory) mucus, cervicovaginal secretions from women with BV, and CVM mixed with semen are important next steps in our understanding of the protective role of female genital mucus secretions against pathogens and when protection may be compromised.

We anticipate that our initial exploration using non-mucoadhesive nanoparticles to observe the effective pore size of CVM will enable further investigations of diverse mucus secretions (e.g., those of the respiratory, gastrointestinal, and reproductive tracts) to determine the pore size and mucoadhesive interactions experienced by viruses and other nanoparticles in those environments.

Materials and Methods

CVM Collection and Preparation. The cervicovaginal mucus collection procedure was performed as published previously (6, 56). Briefly, undiluted cervicovaginal secretions from women with healthy vaginal microflora, averaging 0.3 g per sample, were obtained by using a self-sampling menstrual collection device following protocols approved by the Institutional Review Board of The Johns Hopkins University. The device was inserted into the vagina for approximately 30 s, removed, and placed into a 50-mL centrifuge tube. Samples were centrifuged at 1,000 rpm for 2 min to collect the secretions; cells were not separated from the mucus gel under these settings. Collected mucus was used for microscopy within 4 hr. The samples were collected at random times throughout the menstrual cycle but excluding the midcycle ovulatory interval (none exhibited spinnbarkeit). Samples that were nonuniform in color or consistency were also discarded. All mucus samples used in this study were obtained from donors of reproductive age, ranging from 18- to 27-yr old. Donors stated they had not used vaginal products nor participated in unprotected intercourse within 3 d prior to donating. All samples were pH 3.5–4; none had BV by Nugent score and none were obtained during ovulation based on the absence of spinnbarkeit. We did not detect the presence of IgG antibodies against HSV with ELISA in the samples used to study the transport of HSV. CVM naturally contains sloughed epithelial cells. We were careful not to pellet these cells during mucus collection so as to avoid any potential damage that cell pelleting may cause to the mucus structure.

Preparation and Characterization of Non-Mucoadhesive Particles. Fluorescent, carboxyl-modified polystyrene particles sized 100 nm, 200 nm, 500 nm, and 1 μm (Molecular Probes, Eugene, OR) were covalently modified with 2–3.4-kDa amine-modified PEG (Nektar Therapeutics, San Carlos, CA) via a carboxyl-amine reaction, as published previously (6). Unconjugated PEG was removed by three rounds of washing and centrifugation, and PEG-coated particles were stored at 4 °C until use. A near-neutral ξ-potential, measured by laser Doppler anemometry, was used to confirm PEG conjugation (6). We previously reported that 100-nm PEG-coated particles were greatly slowed in mucus, and suggested that the particles may have been inadequately PEGylated (6). We have since shown that the transport of particles in mucus is critically dependent on the density of PEG on the particle surface (17). This discovery enabled us to prepare 100-nm muco-inert particles for this study that were almost 7,000-fold faster than the 100-nm coated particles from our previous work.

MPT of PEG-Coated Particles in CVM. The trajectories of fluorescent PEG-coated particles in CVM were recorded by using a silicon-intensified target camera (VE-1000, Dage-MTI, Michigan, IN) mounted on an inverted

epifluorescence microscope equipped with a 100× oil-immersion objective (numerical aperture 1.3). Experiments were carried out in 8-well glass chambers (LabTek, Campbell, CA) where diluted particle solutions (approximately 10^{10} particles/mL) were added to 250–500 μL of fresh mucus to a final concentration of <2% vol/vol and incubated for 2 hr prior to microscopy. Immediately after imaging of particles in native mucus, 10% wt/vol (nonylphenoxy)polyethylene oxide (Igepal CO-630, Rhône-Poulenc, Courbevoie, France) was added to a final concentration of 1% vol/vol, gently stirred, and incubated for 2 hr prior to a second round of microscopy. Trajectories of $n > 120$ particles were analyzed for each experiment and at least three experiments in CVM from different donors were performed for each condition. Movies were captured with Metamorph software (Universal Imaging Corp., Downingtown, PA) at a temporal resolution of 66.7 ms for 20 s. The tracking resolution was 10 nm, as determined by tracking the displacements of particles immobilized with a strong adhesive (57). The coordinates of nanoparticle centroids were transformed into time-averaged MSDs, calculated as $\langle \Delta r^2(\tau) \rangle = [x(t+\tau) - x(t)]^2 + [y(t+\tau) - y(t)]^2$ (where $\tau =$ time scale or time lag), from which distributions of MSDs and effective diffusivities (D_{eff}) were calculated, as previously demonstrated (6, 18, 58). The MSD of nanoparticles vs. τ can also be fit to the equation $\text{MSD} = 4D_0\tau^{\alpha}$ to obtain α, the slope of the curve on a log–log scale, which is a measure of the extent of impediment to particle diffusion. Additional information for measuring 3D transport by 2D particle tracking is described in a recent review (18).

Probing the Structural Arrangement of the Mucus Gel Mesh. The pore sizes between mucin fibers of human CVM were estimated based on an obstruction-scaling model pioneered by Amsden and coworkers that was originally developed for covalently cross-linked hydrogels but is equally applicable to gels with physical entanglement cross-links such as mucus (8, 19–21). The model is valid when there is no chemical interaction between solute particles and the gel mesh, and particles traveling through the pores of the gel experience the viscous drag of water. The model describes the ratio of diffusion in a gel and diffusion in water as $D_g/D_o = \exp((-\pi/4)((r_s + r_f)/(r_g + r_f))^2)$, where D_g is the diffusion coefficient of the particle in the polymer gel, D_o is its diffusion coefficient in water, r_s is the particle radius, r_f is the gel fiber radius, and r_g is the effective radius of the pore. An r_f of 3.5 nm was used as the current best estimate for the radius of individual mucin fibers from biochemical, EM, and atomic force microscopy observations (8, 21). The average effective pore size ($2r_g$) was obtained by fitting measured transport data via the maximum likelihood method.

MPT of HSV in CVM. GFP-labeled HSV-1 was constructed and generously provided by P. Desai (Johns Hopkins University). To improve the fluorescence labeling for HSV, we further conjugated AlexaFluor 488 to the surface of the virus at an incubation concentration of 10,000:1 fluorophore to virus for 1 hr, followed by purification via Sephadex G25 spin column based on the principle of size exclusion chromatography. Conjugation of a high density of AlexaFluor 488 on the surface of non-mucoadhesive synthetic particles did not slow down their transport in mucus (visual observation), suggesting the presence of the AlexaFluor label on a particle surface does not mediate adhesion to mucus. Fluorescent virions (approximately 10^8–10^9∇ viral particles/mL) were added to 30 μL of CVM at 3% vol/vol ratio, placed in a custom-made glass chamber, and incubated for 1 hr prior to microscopy. The translational motions of fluorescent virions were recorded by using an electron-multiplying charge-coupled device camera (Cascade II: 512, Photometrics, Tucson, AZ) mounted on an inverted epifluorescence microscope (3-I Marianas, Zeiss, Thornwood, NY) equipped with a 100× oil-immersion objective (numerical aperture 1.3). Movies were captured with Slidebook 4.2 Advanced Imaging Software (Olympus Soft Imaging Corp., Lakewood, CO) at a temporal resolution of 66.7 ms for 20 s. The translational motions were analyzed as described above (9, 10). Three independent experiments in CVM from different donors, with $n > 100$ virions per experiment, were performed for each condition.

ACKNOWLEDGMENTS. We thank the Integrated Imaging Center at Johns Hopkins University, D.E. O'Hanlon for mucus collection, and C.-H. Lee for assistance with analysis of MPT data. Supported in part by the National Institutes of Health Grants 5U01AI066726 (R.C.), R21HL089816 (J.H.), and R01EB00355 (J.H.), and by graduate research fellowships (National Science Foundation for Y.-Y.W.).

1. Cone R (2005) *Mucosal Immunology*, eds Mestecky J, et al. (Academic, San Diego), pp 49–72.
2. Gipson IK (2005) Human endocervical mucins. *Ernst Schering Res Found Workshop* 219–244.
3. Knowles MR, Boucher RC (2002) Mucus clearance as a primary innate defense mechanism for mammalian airways. *J Clin Invest*, 109:571–577.
4. Chilvers MA, O'Callaghan C (2000) Local mucociliary defence mechanisms. *Paediatr Respir Rev*, 1:27–34.
5. Carlstedt I, Sheehan JK (1989) Structure and macromolecular properties of cervical mucus glycoproteins. *Symp Soc Exp Biol*, 43:289–316.
6. Lai SK, et al. (2007) Rapid transport of large polymeric nanoparticles in fresh undiluted human mucus. *Proc Natl Acad Sci USA*, 104:1482–1487.
7. Lai SK, Wang YY, Hanes J (2009) Mucus-penetrating nanoparticles for drug and gene delivery to mucosal tissues. *Adv Drug Deliv Rev*, 61:158–171.
8. Olmsted SS, et al. (2001) Diffusion of macromolecules and virus-like particles in human cervical mucus. *Biophys J*, 81:1930–1937.
9. Lai SK, Wang YY, Wirtz D, Hanes J (2009) Micro- and macrorheology of mucus. *Adv Drug Deliv Rev*, 61:86–100.
10. Saltzman WM, Radomsky ML, Whaley KJ, Cone RA (1994) Antibody diffusion in human cervical mucus. *Biophys J*, 66:508–515.
11. Yudin AI, Hanson FW, Katz DF (1989) Human cervical mucus and its interaction with sperm: A fine-structural view. *Biol Reprod*, 40:661–671.
12. Ceric F, Silva D, Vigil P (2005) Ultrastructure of the human periovulatory cervical mucus. *J Electron Microsc*, 54:479–484.
13. Chretien FC, Cohen J, Borg V, Psychoyos A (1975) Human cervical mucus during the menstrual cycle and pregnancy in normal and pathological conditions. *J Reprod Med*, 14:192–196.
14. Poon WW, McCoshen JA (1985) Variances in mucus architecture as a cause of cervical factor infertility. *Fertil Steril*, 44:361–365.
15. O'Mullane JE, Artursson P, Tomlinson E (1987) Biopharmaceutics of microparticulate drug carriers. *Ann NY Acad Sci*, 507:120–140.
16. Sanders NN, et al. (2000) Cystic fibrosis sputum: A barrier to the transport of nanospheres. *Am J Respir Crit Care Med*, 162:1905–1911.
17. Wang YY, et al. (2008) Addressing the PEG mucoadhesivity paradox to engineer nanoparticles that "slip" through the human mucus barrier. *Angew Chem Int Ed Engl*, 47:9726–9729.
18. Suh J, Dawson M, Hanes J (2005) Real-time multiple-particle tracking: Applications to drug and gene delivery. *Adv Drug Deliv Rev*, 57:63–78.
19. Amsden B (1998) Solute diffusion within hydrogels. Mechanisms and models. *Macromolecules*, 31:8382–8395.
20. Amsden B (1999) An obstruction-scaling model for diffusion in homogeneous hydrogels. *Macromolecules*, 32:874–879.
21. Shen H, Hu Y, Saltzman WM (2006) DNA diffusion in mucus: Effect of size, topology of DNAs, and transfection reagents. *Biophys J*, 91:639–644.
22. Sheehan JK, Oates K, Carlstedt I (1986) Electron microscopy of cervical, gastric and bronchial mucus glycoproteins. *Biochem J*, 239:147–153.
23. Slayter HS, Wold JK, Midtvedt T (1991) Intestinal mucin of germ-free rats. Biochemical and electron-microscopic characterization. *Carbohydr Res*, 222:1–9.
24. Allen A, Flemstrom G, Garner A, Kivilaakso E (1993) Gastroduodenal mucosal protection. *Physiol Rev*, 73:823–857.
25. Carlstedt I, Lindgren H, Sheehan JK, Ulmsten U, Wingerup L (1983) Isolation and characterization of human cervical-mucus glycoproteins. *Biochem J*, 211:13–22.
26. Chao CC, Butala SM, Herp A (1988) Studies on the isolation and composition of human ocular mucin. *Exp Eye Res*, 47:185–196.
27. Quraishi MS, Jones NS, Mason J (1998) The rheology of nasal mucus: A review. *Clin Otolaryngol Allied Sci*, 23:403–413.
28. Samet JM, Cheng PW (1994) The role of airway mucus in pulmonary toxicology. *Environ Health Perspect*, 102(Suppl 2):89–103.
29. Biehl R, et al. (2004) Diffusion of compact macromolecules through polymer meshes: Mesh dynamics and probe dynamics. *Phys B*, 350:76–78.
30. Sheehan JK, Carlstedt I (1984) Hydrodynamic properties of human cervical-mucus glycoproteins in 6M-guanidinium chloride. *Biochem J*, 217:93–101.
31. Lai SK, Wang YY, Cone R, Wirtz D, Hanes J (2009) Altering mucus rheology to "solidify" human mucus at the nanoscale. *PLoS One*, 4:e4294.
32. Slomiany BL, Tsukada H, Slomiany A (1986) Cotranslational attachment of fatty acids to nascent peptides in gastric mucus glycoprotein. *Biochem Biophys Res Commun*, 141:387–393.
33. Brunelli R, et al. (2007) Globular structure of human ovulatory cervical mucus. *FASEB J*, 21:3872–3876.
34. Cao X, et al. (1999) pH-dependent conformational change of gastric mucin leads to sol-gel transition. *Biophys J*, 76:1250–1258.
35. Hong Z, et al. (2005) Atomic force microscopy reveals aggregation of gastric mucin at low pH. *Biomacromolecules*, 6:3458–3466.
36. Lai SK, et al. (2009) HIV is trapped by acidic but not by neutralized human cervicovaginal mucus. *J Virol*.
37. Cone RA (2009) Barrier properties of mucus. *Adv Drug Deliv Rev*, 61:75–85.
38. Girod S, Zahm JM, Plotkowski C, Beck G, Puchelle E (1992) Role of the physiochemical properties of mucus in the protection of the respiratory epithelium. *Eur Respir J*, 5:477–487.
39. King M (2006) Physiology of mucus clearance. *Paediatr Respir Rev*, 7(Suppl 1): S212–214.
40. Rubin BK (2007) Mucus structure and properties in cystic fibrosis. *Paediatr Respir Rev*, 8:4–7.
41. Shirazi T, Longman RJ, Corfield AP, Probert CS (2000) Mucins and inflammatory bowel disease. *Postgrad Med J*, 76:473–478.
42. Cone RA, et al. (2006) Vaginal microbicides: Detecting toxicities in vivo that paradoxically increase pathogen transmission. *BMC Infect Dis*, 6:90.

43. Galen BT, et al. (2007) A comprehensive murine model to evaluate topical vaginal microbicides: Mucosal inflammation and susceptibility to genital herpes as surrogate markers of safety. *J Infect Dis*, 195:1332–1339.
44. Phillips DM, Zacharopoulos VR (1998) Nonoxynol-9 enhances rectal infection by herpes simplex virus in mice. *Contraception*, 57:341–348.
45. Van Damme L, et al. (2002) Effectiveness of COL-1492, a nonoxynol-9 vaginal gel, on HIV-1 transmission in female sex workers: A randomised controlled trial. *Lancet*, 360:971–977.
46. Haines-Butterick L, et al. (2007) Controlling hydrogelation kinetics by peptide design for three-dimensional encapsulation and injectable delivery of cells. *Proc Natl Acad Sci USA*, 104:7791–7796.
47. Suk JS, et al. (2009) The penetration of fresh undiluted sputum expectorated by cystic fibrosis patients by non-adhesive polymer nanoparticles. *Biomaterials*, 30:2591–2597.
48. Matsui H, et al. (2005) Reduced three-dimensional motility in dehydrated airway mucus prevents neutrophil capture and killing bacteria on airway epithelial surfaces. *J Immunol*, 175:1090–1099.
49. Fleming DT, et al. (1997) Herpes simplex virus type 2 in the United States, 1976 to 1994. *N Engl J Med*, 337:1105–1111.
50. Mbopi-Keou FX, et al. (2000) Interactions between herpes simplex virus type 2 and human immunodeficiency virus type 1 infection in African women: Opportunities for intervention. *J Infect Dis*, 182:1090–1096.
51. Allsworth JE, Peipert JF (2007) Prevalence of bacterial vaginosis: 2001–2004 National Health and Nutrition Examination Survey data. *Obstet Gynecol*, 109:114–120.
52. Olmsted SS, Meyn LA, Rohan LC, Hillier SL (2003) Glycosidase and proteinase activity of anaerobic gram-negative bacteria isolated from women with bacterial vaginosis. *Sex Transm Dis*, 30:257–261.
53. Martin HL, et al. (1999) Vaginal lactobacilli, microbial flora, and risk of human immunodeficiency virus type 1 and sexually transmitted disease acquisition. *J Infect Dis*, 180:1863–1868.
54. Taha TE, et al. (1998) Bacterial vaginosis and disturbances of vaginal flora: Association with increased acquisition of HIV. *AIDS*, 12:1699–1706.
55. Cherpes TL, Meyn LA, Krohn MA, Lurie JG, Hillier SL (2003) Association between acquisition of herpes simplex virus type 2 in women and bacterial vaginosis. *Clin Infect Dis*, 37:319–325.
56. Boskey ER, Moench TR, Hees PS, Cone RA (2003) A self-sampling method to obtain large volumes of undiluted cervicovaginal secretions. *Sex Transm Dis*, 30:107–109.
57. Apgar J, et al. (2000) Multiple-particle tracking measurements of heterogeneities in solutions of actin filaments and actin bundles. *Biophys J*, 79:1095–1106.
58. Dawson M, Wirtz D, Hanes J (2003) Enhanced viscoelasticity of human cystic fibrotic sputum correlates with increasing microheterogeneity in particle transport. *J Biol Chem*, 278:50393–50401.